ELSEVIER

Journal of Magnetism and Magnetic Materials 153 (1996) 35–49

journal of magnetism and magnetic materials

Grain-size dependence of remanence and coercive field of isotropic nanocrystalline composite permanent magnets

R. Fischer [a], T. Schrefl [a,b], H. Kronmüller [a,*], J. Fidler [b]

[a] *Max-Planck-Institut für Metallforschung, Institut für Physik, Postfach 80 06 65, 70506 Stuttgart, Germany*
[b] *Institut für Angewandte und Technische Physik, T.U. Wien, Wiedner Hauptstraße 8, A-1040 Vienna, Austria*

Received 30 January 1995; revised 3 July 1995

Abstract

Micromagnetic calculations using a finite element technique are useful to investigate magnetization processes in nanocrystalline ferromagnetic materials. In particular numerical calculations reveal the microstructural conditions required for high remanence and high coercivity isotropic permanent magnets. composite materials of $Nd_2Fe_{14}B$ and α-Fe are excellent candidates for such high performance permanent magnets. The soft magnetic α-Fe grains cause a large spontaneous magnetization and the hard magnetic grains induce a large coercive field, provided that both phases are strongly exchange coupled. The numerical investigations on realistic three-dimensional grain arrangements suggest an optimal microstructure consisting of small soft magnetic grains ($D \approx 10$ nm, $V^{soft} \approx 40\%$) embedded between hard magnetic grains with a mean grain diameter of about $D \approx 20$ nm. Additionally, a microstructure with regular shaped grains improves the magnetic properties.

1. Introduction

The magnetic properties of isotropic nanocrystalline two-phase permanent magnets depend sensitively on microstructural features, such as the distribution of the magnetically hard and soft phase, the average grain size, the particle shape and the grain boundary type. Numerical micromagnetic calculations using a finite element technique provide a deeper understanding of the relation between the grain structure and the magnetic properties such as the remanence J_r, the coercive field H_c and the maximum energy product $(BH)_{max}$. Here $B = \mu_0 H + J$ denotes the flux density and $H = H_{ext} + H_d$ is the internal field of the permanent magnet in the second quadrant of the hysteresis loop. The internal field H is the sum of the external opposite field H_{ext} (< 0) and the macroscopic demagnetizing field H_d. In the case of a magnet of cubic shape H_d can be approximately written as $H_d \approx -\frac{1}{3}(J/\mu_0)$. In order to obtain high maximum energy products, it is necessary to increase the remanence and keep the coercive field sufficiently high [1]. Additionally, the hysteresis loop should be as rectangular as possible. Therefore, the maximum energy product is a useful measure of the performance of a particular permanent magnet. Whereas in conventional magnets, such as Alnico or Ba-ferrites the characteristic energy products are of the order of $(BH)_{max} \leq 50$ kJ/m^3, for rare earth-transition metal intermetallic compounds, the maximum energy products have been increased above 300 kJ/m^3 for laboratory magnets. A further increase of the maximum energy product is possible

* Corresponding author. Fax: +49-711-6891932.

SSDI 0304-8853(95)00494-7

in isotropic nanocrystalline composite magnets if the grain structure consists of small soft and hard magnetic grains without any grain boundary phases separating adjacent grains [2–7]. As described below, such isotropic two-phase permanent magnets show remarkably high maximum energy products of about 400 kJ/m^3 owing to remanence enhancement and exchange hardening.

For isotropic permanent magnets with noninteracting homogeneously magnetized single domain particles, the ratio of the remanence J_r to the saturation polarization J_{sat} is identical to the theoretical limit 0.5, given by the Stoner–Wohlfarth theory [8]. Actually, nanocrystalline isotropic permanent magnets show in general an enhanced remanence $J_r \geq 0.5 J_{sat}$. This so-called remanence enhancement is entirely attributed to intergrain exchange interactions [9,10]. The coercive field is also sensitively influenced by exchange interactions. But additionally, dipolar interactions can play an important role [11,12]. Therefore a theoretical treatment of magnetization reversal processes must take into account both short-range exchange interaction and long-range dipolar interactions. These particle interactions are an inherent part of the simulation model, which rigorously describes the magnetic behaviour of real three-dimensional magnets. Since the simulation model relies only on micromagnetic concepts and does not introduce any artificial assumptions, the numerical results allow an understanding of the relation between microstructural features and magnetic properties within the framework of micromagnetism. Two-dimensional calculations have been performed previously [13].

The present article deals exclusively with three-dimensional grain structures and is organized as follows: Section 2 describes the micromagnetic background of the simulations model. Section 3 presents numerical results for the grain-size dependence of the remanence and coercive field for two different grain structures. Finally, Section 4 compares the derived numerical values with experimental results.

2. Micromagnetic background

Micromagnetism is a continuum theory to describe the orientation of the spontaneous magnetic polarization J_s in ferromagnetic bodies [14,15]. The

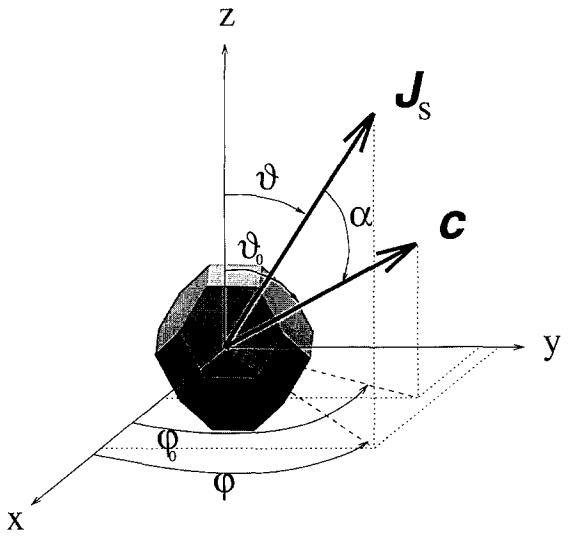

Fig. 1. Spherical coordinates of the spontaneous magnetic polarization (ϑ,φ) and the easy axis (ϑ_0,φ_0) of a particular grain.

significant length scales are small enough to reveals details of transition regions between domains and large enough to approximate the direction angles of the atomic spins with continuous functions of position [16,17]. The basic concept of micromagnetism is the introduction of the spontaneous magnetic polarization J_s, whose modulus is independent of an applied field. A stable equilibrium state of $J_s(r)$ can be obtained by minimizing the total Gibbs free energy Φ_t with respect to the spontaneous magnetic polarization, subject to the constraint $|J_s| = J_s =$ constant. For numerical micromagnetic calculations it is more convenient to express J_s in spherical coordinates ϑ and φ according to Fig. 1. If magnetoelastic and surface anisotropy effects are neglected, the magnetic Gibbs free energy for uniaxial magnetic materials is given by:

$$\Phi_t[J_s(\vartheta(r),\varphi(r))] = \int d^3r \Big\{ A\big((\nabla\vartheta(r))^2 + (\nabla\varphi(r))^2 \sin^2\vartheta(r)\big) \tag{1}$$

$$+K_1 \sin^2\alpha(\vartheta(r),\varphi(r)) \tag{2}$$

$$+K_2 \sin^4\alpha(\vartheta(r),\varphi(r)) \tag{3}$$

$$-J_s(\vartheta(r),\varphi(r)) \cdot H_{ext} \tag{4}$$

$$-\frac{1}{2\mu_0} J_s(\vartheta(r),\varphi(r)) \cdot H_s(\vartheta(r),\varphi(r)) \Big\}$$

where the terms in (1)–(4) represent the exchange energy, the anisotropy energy, the magnetostatic energy, and the stray-field energy, respectively, with K_1, K_2 the anisotropy constants and A the exchange constant. The stray field $\boldsymbol{H}_s$ arises from magnetic volume charges $\nabla \cdot \boldsymbol{J}_s$ within the grains and magnetic surface charges $\boldsymbol{J}_s \cdot \boldsymbol{n}$ at the grain boundaries ($\boldsymbol{n}$ is the surface normal). The angle α between the spontaneous magnetic polarization $\boldsymbol{J}_s$ and the easy axes c is given by (see Fig. 1)

$$\cos \alpha = \frac{\boldsymbol{J}_s \cdot \boldsymbol{c}}{|\boldsymbol{J}_s||\boldsymbol{c}|}, \tag{5}$$

and therefore depends on ϑ and φ. The repeated calculation of equilibrium states for decreasing external fields H_{ext} provides the demagnetization curve of the ferromagnetic body. For numerical calculations using the finite element method, Brown's vector potential formulation of the micromagnetic problem [14] proved to be the most suitable [18]. A detailed description of the numerical algorithms used for the calculations can be found in [12,19].

The theory of micromagnetism allows an investigation of transition regions between domains. The extension of such transition regions depends sensitively on the material parameters A, K_1 and J_s. In

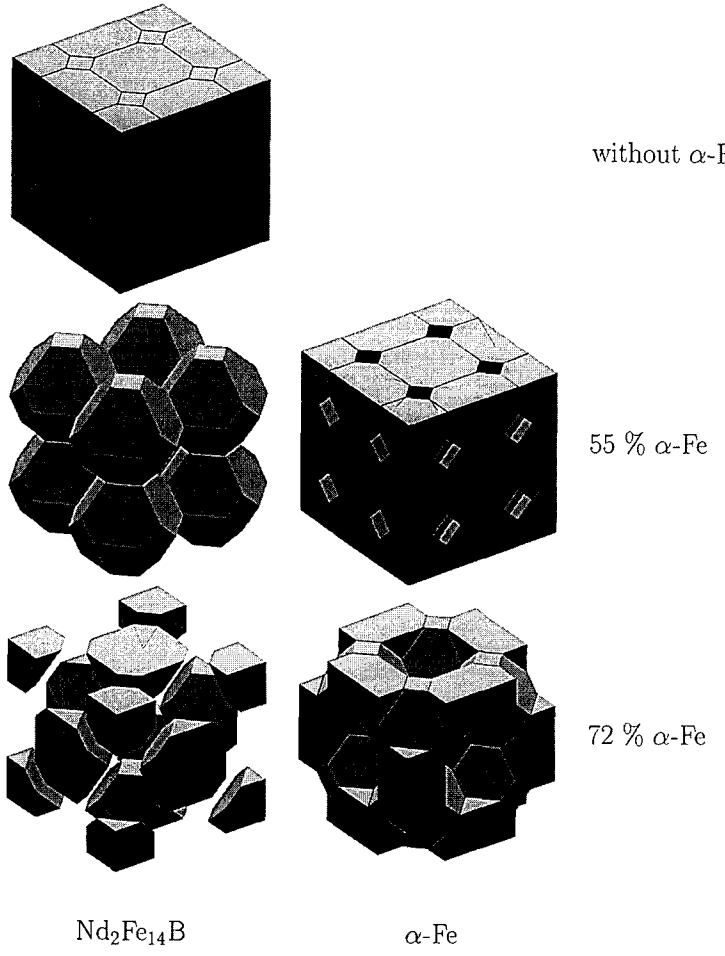

Fig. 2. Three-dimensional model magnets, which consists of 35 regular shaped particles. The complete model magnet results from adding the $Nd_2Fe_{14}B$ grains (left) and α-Fe grains (right). Top: without α-Fe, middle: 55% α-Fe, bottom: 72% α-Fe. The grain diameter is defined by the diameter of a sphere with equal volume.

the limit of small stray-field energy or small anisotropy energy, the range of spin inhomogeneities is determined by two well-known characteristic lengths related to the crystal anisotropy and to the stray-field energy. In hard magnetic materials, the anisotropy energy overrides in general the stray-field energy. In this case, the extension of spin inhomogeneities is given by the so-called exchange length of the crystal anisotropy

$$l_K \equiv \sqrt{\frac{A}{K_1}} . \tag{6}$$

The wall width of 180°-domain walls is related to l_K by $\delta_B = \pi l_K$. The situation changes in soft magnetic materials with a low magnetocrystalline anisotropy. Here, the exchange length

$$l_s \equiv \sqrt{\frac{\mu_0 A}{J_s^2}} \tag{7}$$

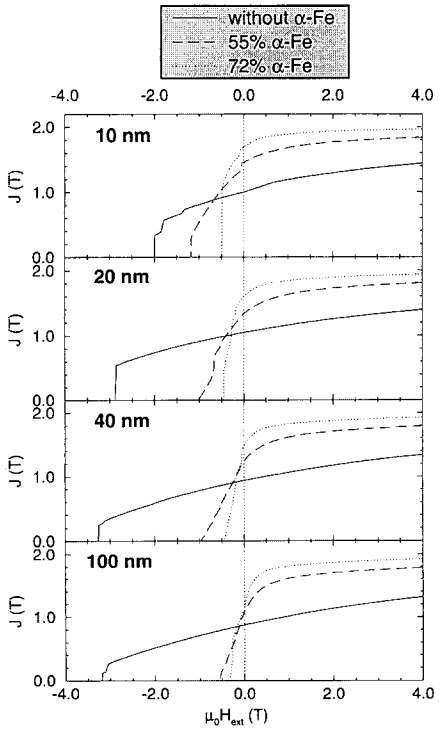

Fig. 3. Demagnetization curves of isotropic, $Nd_2Fe_{14}B$-based composite magnets containing 0% (solid lines), 55% (dashed lines), and 72% α-Fe (dotted lines).

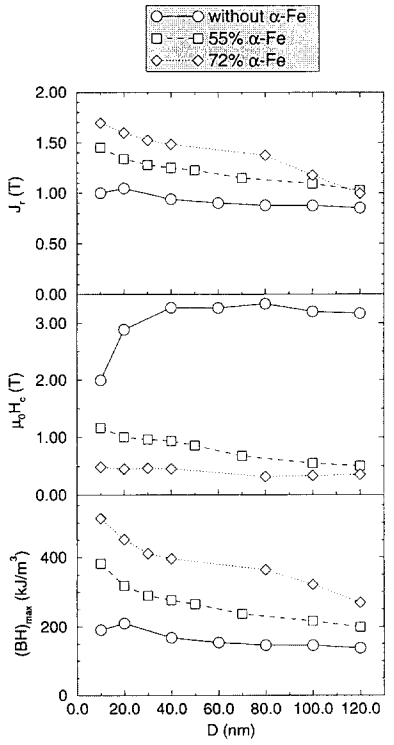

Fig. 4. Remanence J_r, coercive field $\mu_0 H_c$ and maximum energy product $(BH)_{max}$ of the regular grain arrangements of Fig. 2 as a function of the mean grain size D.

corresponds to the lower limit of the range of spin inhomogeneities. It turns out that the quantities πl_K and πl_s are very useful for an understanding of the dependence of the magnetic properties, such as remanence and coercive field, on the mean grain diameter for nanocomposite magnetic materials.

3. Grain-size dependence of magnetic properties

3.1. Regular grain structure

Fig. 2 presents the grain structure used for the investigation of the grain-size dependence of remanence and coercive field in isotropic nanocrystalline permanent magnets. It is assumed that each grain is a uniaxial particle. Furthermore the 35 grains are in direct contact without any grain boundary phases. In order to describe composite magnets, material pa-

rameters for magnetically hard and soft phases are assigned to each grain. For the calculations the material parameters for $Nd_2Fe_{14}B$ ($K_1 = 4.3 \times 10^6$ J/m^3, $K_2 = 0.65 \times 10^6$ J/m^3, $A = 7.7 \times 10^{-12}$ J/m, $J_s = 1.63$ T) [20] and α-Fe ($K_1 = 4.6 \times 10^4$ J/m^3, $K_2 = 1.5 \times 10^4$ J/m^3, $A = 2.5 \times 2.5^{-11}$ J/m, $J_s = 2.15$ T) [21] at $T = 300$ K have been used. Fig. 2 shows the hard and soft magnetic grains of the investigated grain structures with 0%, 55% and 72% α-Fe. Both two-phase magnets result from adding the $Nd_2Fe_{14}B$ and α-Fe grains. The average grain size has been varied between 10 nm and 120 nm.

The demagnetization curves, presented in Fig. 3, show the magnetic properties of the isotropic permanent magnet with regular shaped grains for different grain diameters and 0% (solid lines), 55% (dashed lines) and 72% (dotted lines) α-Fe contents. The dependence of the remanence J_r, the coercive field H_c and the maximum energy product $(BH)_{max}$ on grain size is shown in Fig. 4. Independently of the volume fraction of the soft magnetic phase, the remanence decreases with increasing grain size. This is not necessarily true for the coercive field. If the α-Fe percentage is small, the coercive field can increase with increasing grain size for small grains between 10 and 50 nm. According to Fig. 4, highly remanent composite magnets show low coercive fields compared to $Nd_2Fe_{14}B$ magnets without α-Fe. Nevertheless, two-phase permanent magnets with 55% α-Fe exhibit a large maximum energy product of about 400 kJ/m^3 if the mean grain diameter is lower than 20 nm.

3.1.1. Remanence

According to the Stoner–Wohlfarth theory [8], which assumes noninteracting homogeneously magnetized single domain particles, an isotropic permanent magnet has a remanence of

$$J_r = \tfrac{1}{2} J_{sat} \tag{8}$$

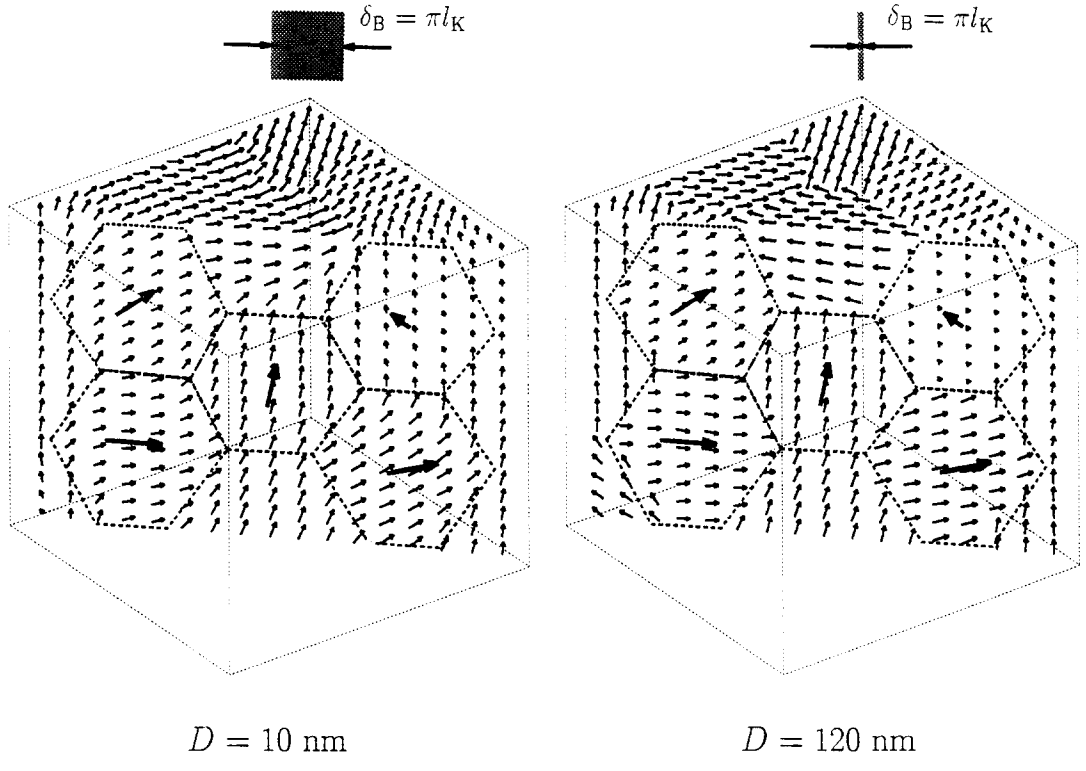

Fig. 5. Distribution of the spontaneous magnetic polarization ($H_{ext} = 0$) for an isotropic nanocrystalline $Nd_2Fe_{14}B$ magnet with 35 regular shaped grains and a mean grain diameter D of about 10 and 120 nm, respectively. All arrows have the same arbitrary length. The dotted lines indicate the grain boundaries and the big strong arrows are the easy axes ($\pi l_K \approx 4.2$ nm).

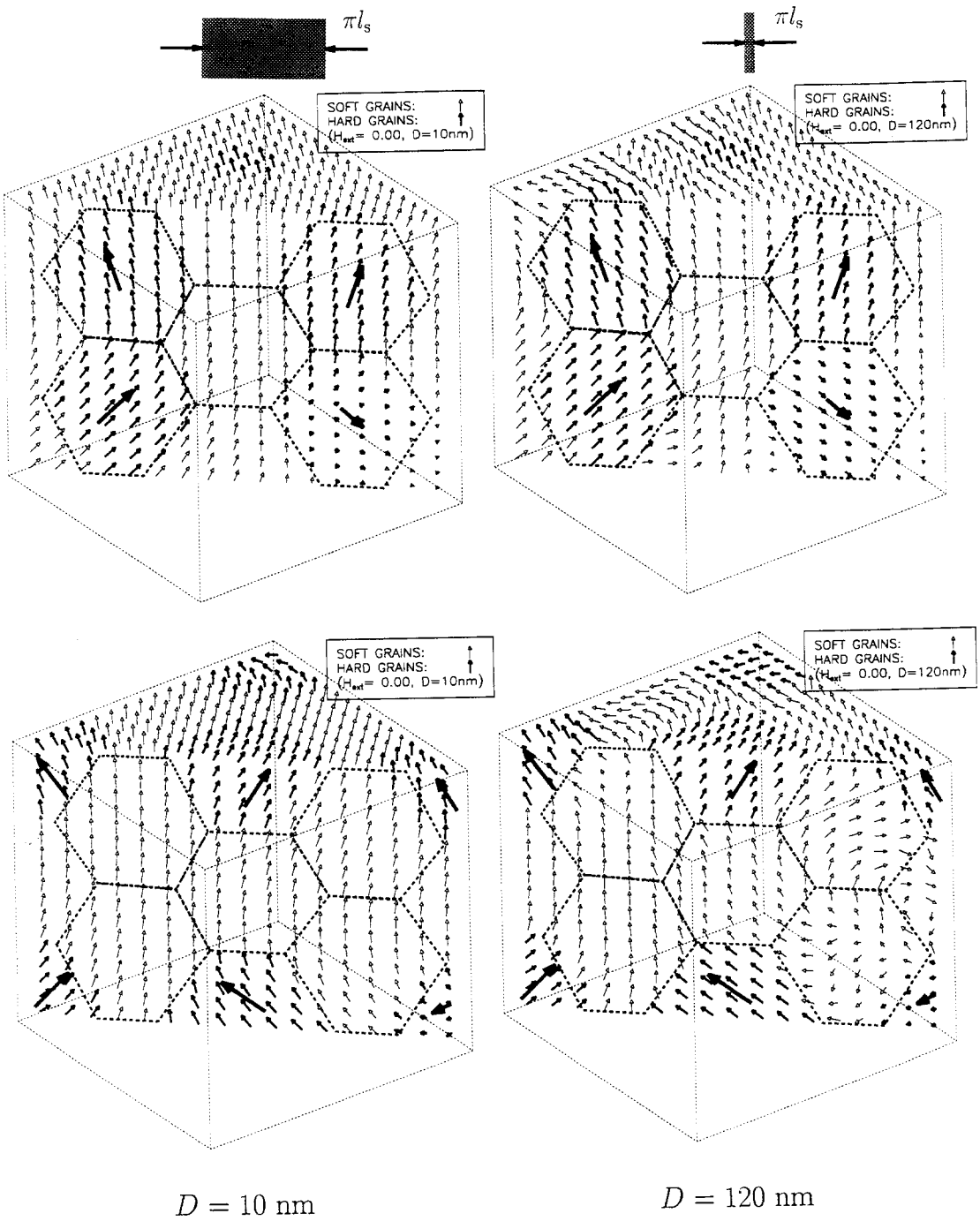

Fig. 6. The same as in Fig. 5, but now for isotropic two-phase permanent magnets containing 51% (top) and 72% α-Fe (bottom). For mean grain sizes of about 10 nm, the exchange interaction couples the soft magnetic moments completely to the hard magnetic grains. The strong arrows belong to the hard magnetic phase and the weak ones to the soft magnetic phase ($\pi l_s \approx 8.2$ nm).

for all grain sizes (see dotted line in Fig. 10). However, the numerically derived results suggest a logarithmic dependence of J_r on the average grain size D. The following empirical laws can be found: without α-Fe:

$$J_r = J_{sat}\{0.6854 - 0.0454 \cdot \ln(D/\delta_B^{hard})\}, \quad (9)$$

with 55% α-Fe:

$$J_r = J_{sat}\{0.8390 - 0.0851 \cdot \ln(D/\delta_B^{hard})\}, \quad (10)$$

with 72% α-Fe:

$$J_r = J_{sat}\{0.9917 - 0.1245 \cdot \ln(D/\delta_B^{hard})\}. \quad (11)$$

Here J_{sat} corresponds to the volume average of the polarization of ideally oriented hard and soft grains with volume fractions v^{hard} and v^{soft}

$$J_{sat} = J_s^{hard} v^{hard} + J_s^{soft} v^{soft} = \begin{cases} 1.61\,T & \text{for } 0\% \text{ α-Fe}, \\ 1.91\,T & \text{for } 55\% \text{ α-Fe}, \\ 2.00\,T & \text{for } 72\% \text{ α-Fe}, \end{cases} \quad (12)$$

and δ_B^{hard} denotes the domain wall width (6) of the hard magnetic $Nd_2Fe_{14}B$-phase:

$$\delta_B = \pi\sqrt{\frac{A}{K_1}} \approx 4.2\,nm. \quad (13)$$

The relation between the remanence and the average grain size for different volume fractions of the soft magnetic phase can be understood by comparing the distribution of the spontaneous magnetic polarization J_s as a function of the average grain size. Fig. 5 clearly demonstrates the effect of the exchange interaction on the distribution of J_s for the $Nd_2Fe_{14}B$ magnet with grain sizes of about 10 and 120 nm, respectively. The interparticle exchange interactions cause a smooth transition of J_s from one easy axis direction to the other near interfaces between grains with different orientations. Only the magnetic moments, which deviate from their easy axes, can increase the resultant polarization parallel to the field direction compared to the remanence of isolated particles. Since the width of the inhomogeneous magnetic states of hard magnetic $Nd_2Fe_{14}B$ is comparable with the domain wall width $\delta_B \approx 4.2$ nm (shaded areas in Fig. 5), the volume fraction of these inhomogeneities becomes smaller for larger grains. Therefore, the remanence enhancement is less significant for grain sizes above 100 nm. The remanence of isotropic nanocrystalline permanent magnets decreases with increasing grain size. According to Figs. 3 or 4, the remanence of two-phase magnets is generally greater than the remanence of the $Nd_2Fe_{14}B$ magnet. In soft magnetic grains with a large spontaneous magnetic polarization, the magnetic moments rotate out of the easy axis more easily than in hard magnetic particles. Since the range of exchange interaction of α-Fe is twice of that of $Nd_2Fe_{14}B$, Fig. 6 shows a good alignment of the soft magnetic moments for an average grain diameter of about 10 nm. Nearly all magnetic moments of the soft magnetic phase align parallel to the average direction of the easy axis of the neighbouring hard magnetic grains. The exchange interaction suppresses stray-field effects such as vortex states or domain structures. But with increasing grain diameter, the exchange hardening of the soft magnetic grains begin to fail and the remanence finally decreases.

3.1.2. Coercive field

The coercive field H_c depends sensitively on microstructural features such as the mean grain size, the distribution and volume fraction of the soft magnetic phase, the particle shape and the orientation of the easy axes. The influence of the mean grain size on the coercive field for different volume fractions of the soft magnetic phase shows the middle part of Fig. 4. Without grains of α-Fe, the coercive field increases for small grains between 10 and 50 nm. This behaviour changes completely with increasing α-Fe contents. If the volume fraction of soft magnetic phase exceeds 50%, the coercive field decreases smoothly with increasing average grain diameter. Consequently, the magnetization reversal process is modified with increasing volume fraction of soft magnetic phase.

3.1.2.1. Magnetization reversal in exchange-coupled NdFeB magnets. In nanoscaled permanent magnets, the exchange coupling between neighbouring grains plays an important role during the demagnetization process. Several studies [22–25] show that the reduction of the exchange coupling between neighbouring hard magnetic grains by grain boundary phases leads

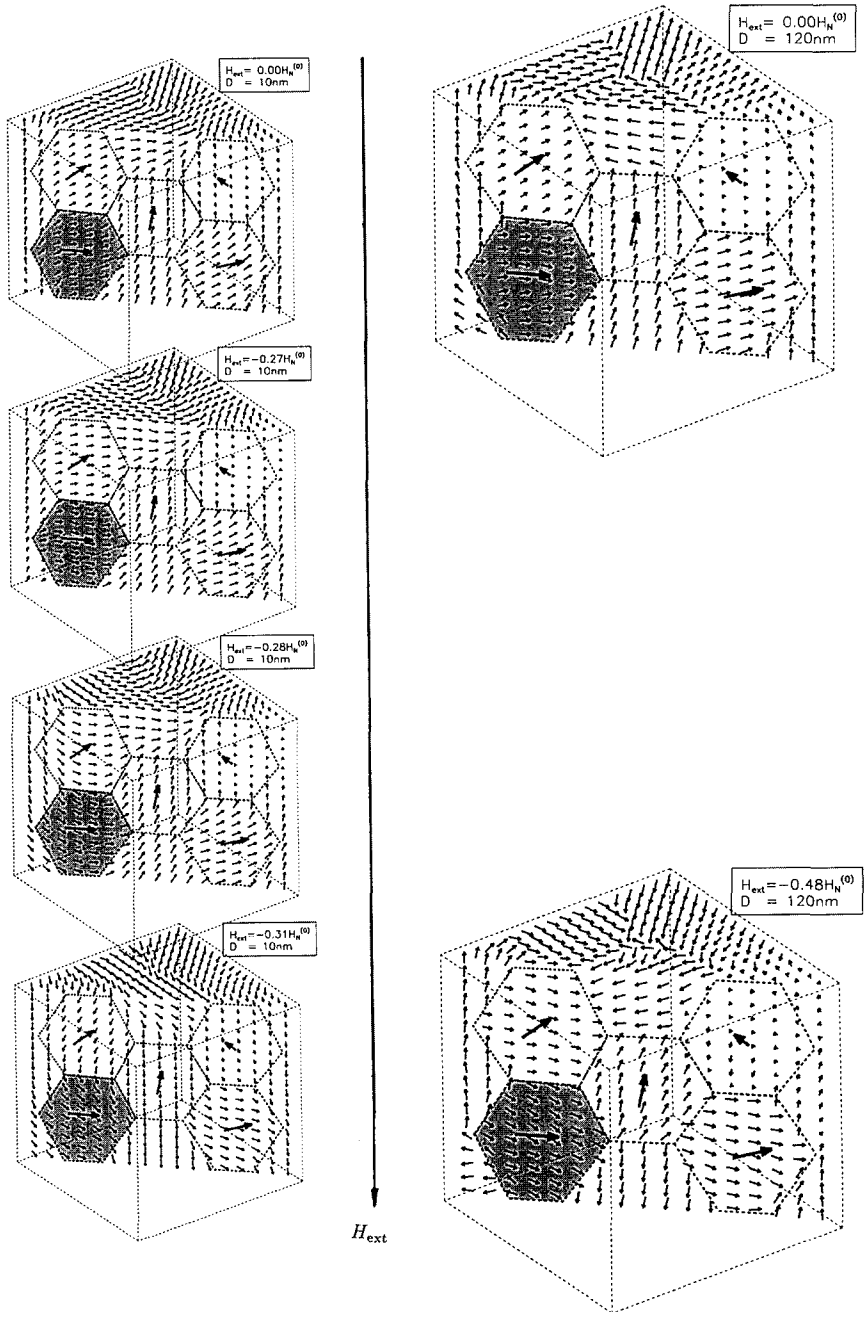

Fig. 7. Distribution of the spontaneous magnetic polarisation for an isotropic $Nd_2Fe_{14}B$ magnet with regular shaped grains. The external field (see boxes) is given in units of $H_N^{(0)} = 2K_1/J_s$. The dotted lines indicate the grain boundaries and the big strong arrows are the easy axes. The shaded grain is an extremely disoriented one. This figure shows the demagnetization process of NdFeB magnets with a mean grain diameter of about 10 nm (left-hand side) and 120 nm (right-hand side).

to an increase of the coercive field. The same effect is obtained by increasing the mean grain diameter, because the range of exchange interaction is of the order of $\delta_B = \pi l_K = 4.2$ nm. According to numerical and experimental investigations (see Fig. 12), the coercive field increases with increasing mean grain diameter until the range of exchange interaction between neighbouring grains becomes much smaller

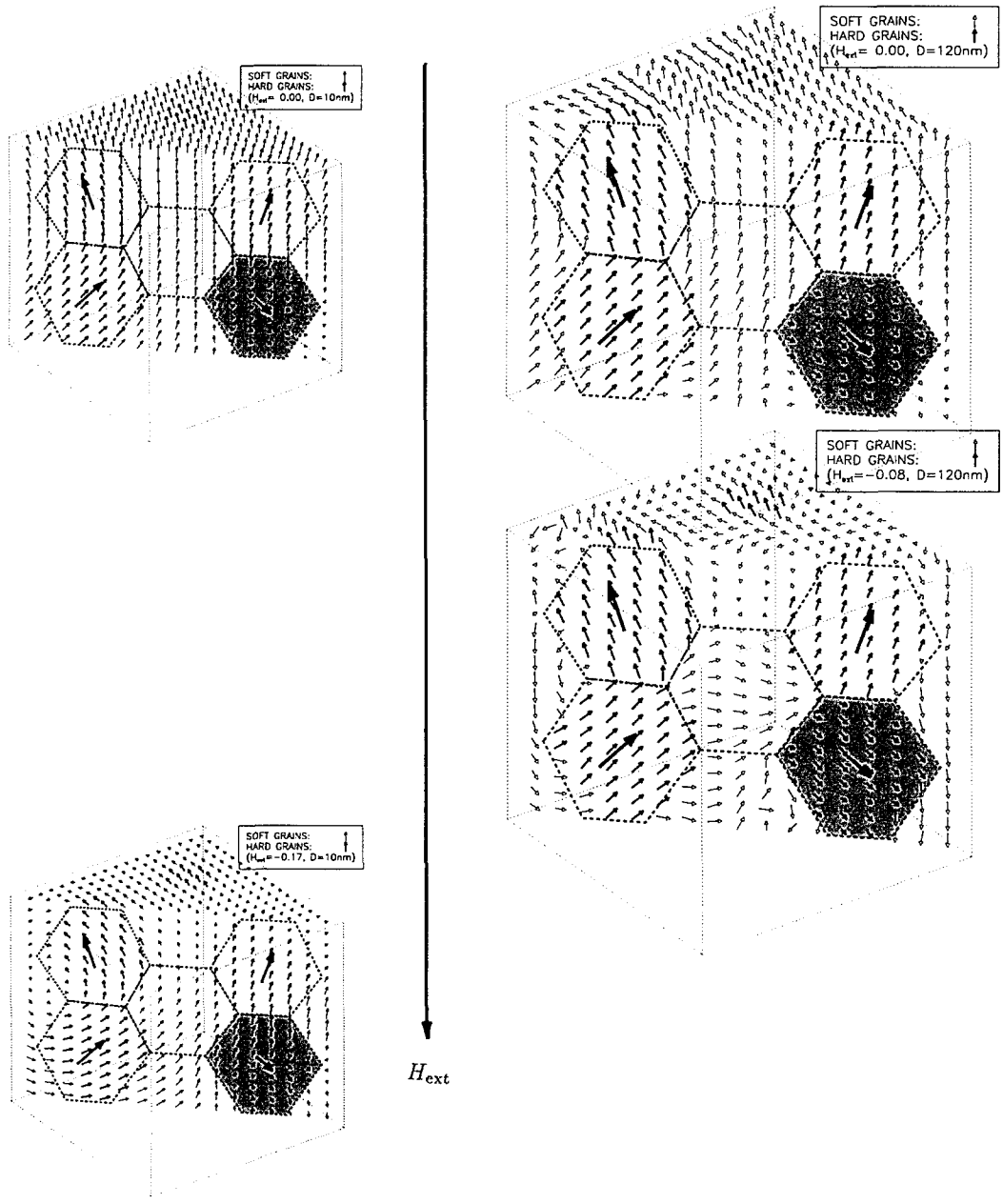

Fig. 8. The same as in Fig. 7, but now for an isotropic two-phase permanent magnet with 51% α-Fe. The strong arrows belong to the hard magnetic phase and the weak ones to the soft magnetic phase. This figure shows the demagnetization process of composite magnets with a mean grain diameter of about 10 nm (left-hand side) and 120 nm (right-hand side).

than the grain size. Therefore, short-range exchange interactions reduce the coercive field in nanoscaled permanent magnets as demonstrated by Figs. 4 and 12.

Numerical investigations of the magnetization reversal process provide a deeper understanding of the deteriorating effect of the exchange coupling between adjacent hard magnetic grains. Fig. 7 shows several snapshots of the magnetization distribution during the demagnetization process. On the left-hand side for a mean grain size of about 10 nm and on the right-hand side of about 120 nm. The shaded grain is extremely disoriented with an angle near 80° between the easy axes and the z-axis. With increasing external field, the magnetic moments of the shaded grain turns more and more out off the easy axes in the H_{ext} direction. For small grains (left-hand side of Fig. 7) the short-range exchange interactions between the shaded and the neighbouring grains induce a reversal of magnetization of the neighbours. At $H_{ext} = -0.31 H_N^{(0)} = -2.05$ T, all neighbours of the disoriented grain have reversed their magnetization direction. With increasing grain diameter and therefore decreasing influence of the exchange coupling between adjacent grains, this effect on the magnetic environment vanishes (right-hand side of Fig. 7). The magnetization reversal than takes place at a greater external field $H_{ext} = -0.48 H_N^{(0)} = -3.18$ T.

3.1.2.2. Magnetization reversal in exchange-coupled NdFeB / α-Fe magnets. Because of the small magnetocrystalline anisotropy, large soft magnetic grains cause magnetization reversal [26,27,19]. This can be avoided due to exchange hardening of sufficiently small soft magnetic grains by adjacent hard magnetic grains. In contrast to pure NdFeB magnets, short-range exchange interactions between neighbouring soft and hard magnetic particles of composite magnets are desired to preserve a high coercive field. Since the range of exchange interaction in soft magnetic particles is of the order of $\pi l_s = 8.2$ nm, the coercive field decreases with increasing mean grain diameter. The following empirical logarithmic laws can be found:

$$H_c = H_N^{(0)}\{0.2203 - 0.0410 \cdot \ln(D/\delta_B^{hard})\} \qquad (14)$$

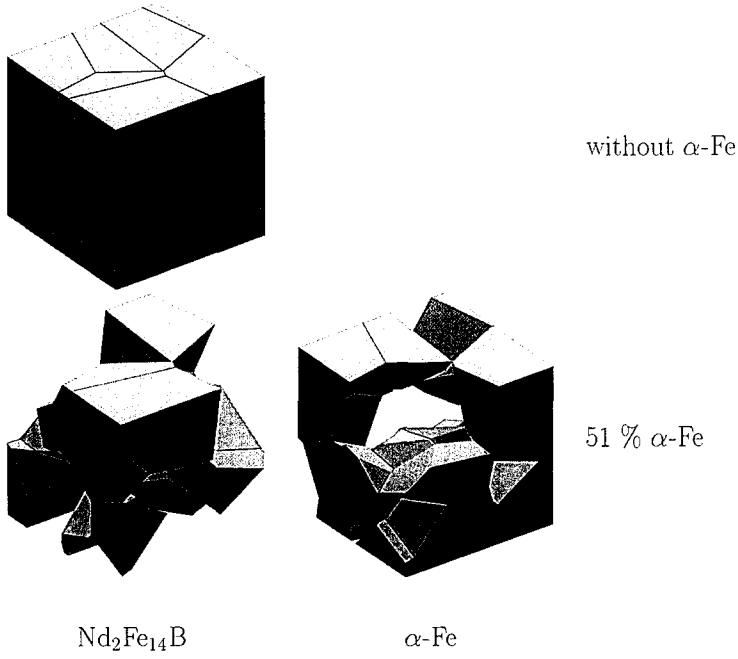

Fig. 9. Three-dimensional model magnets, which consists of 35 irregular shaped particles. The complete model magnet results from adding the $Nd_2Fe_{14}B$ grains (left) and α-Fe grains (right). Top: without α-Fe, bottom: 51% α-Fe.

for 55% α-Fe, and

$$H_c = H_N^{(0)}\{0.0856 - 0.0104 \cdot \ln(D/\delta_B^{hard})\} \quad (15)$$

for 72% α-Fe. Here $H_N^{(0)}$ denotes the ideal nucleation field of the hard magnetic phase and is given by:

$$H_N^{(0)} = \frac{2K_1}{J_s} \approx 6.63\,\mathrm{T}. \quad (16)$$

Therefore, an ideal two-phase magnet consist of small soft magnetic particles embedded between hard magnetic grains without any intergranular phases.

Fig. 8 shows the same as Fig. 7, but now for the NdFeB magnet with 55% α-Fe contents. The shaded grain is extremely disoriented. For small grains of about 10 nm (left-hand side of Fig. 8), the soft magnetic particles in the neighbourhood of the hard magnetic grains are exchange-hardened: The magnetization direction of a soft magnetic grain is the same as the average magnetization directions of all hard magnetic neighbours. This situation changes with increasing mean grain diameter. For grains of about 120 nm (right-hand side of Fig. 8), the exchange hardening by the hard magnetic neighbours is less effective. With increasing external field, the soft magnetic particles reverse their magnetization direction independently of the hard magnetic environment. Therefore, the coercive field decreases with increasing mean grain diameter for composite magnets. One further detail about the demagnetization process in two-phase magnets is interesting: The extremely disoriented grain (shaded one) causes no magnetization reversal of all neighbouring grains as in the case of pure NdFeB magnets. The magnetization direction of the soft grains is always the mean magnetization direction of all hard magnetic grains around the soft magnetic particle and not only of the shaded one.

3.2. Irregular grain structure

The numerical investigation of the grain structure, presented in Fig. 9, allows a comparison of the magnetic properties of microstructures with regular and irregular shaped grains. In the case of the irregular three-dimensional grain structure, there exist sharp edges and corners. Furthermore both grain structures

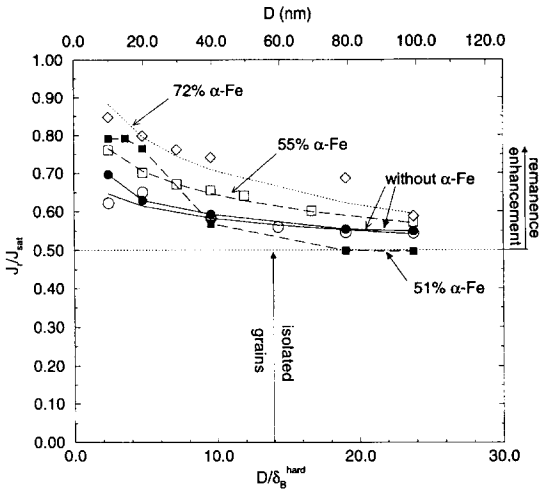

Fig. 10. Reduced remanence J_r/J_{sat} as a function of the mean grain size. The saturation polarization J_{sat} is given by Eq. (12). Within the framework of the Stoner–Wohlfarth theory, which assumes noninteracting single domain particles, the remanence is given by the dotted line (see Eq. (8)). The filled signs belong to the irregular grain structure and the open signs to the regular ones. The lines connecting the open signs are logarithmic fits (see Eqs. (9)–(11)).

differ strongly in their phase distributions. The magnetically soft phase of the regular grain arrangement with 51% α-Fe are more uniformly distributed between the hard magnetic grains than those of the irregular microstructure with 55% α-Fe. As a consequence the two-phase permanent magnet with irregularly shaped grains possess (1) larger extended magnetic grains, and (2) more directly contacted faces between hard magnetic grains as compared to the uniform grain arrangement.

3.2.1. Remanence

Fig. 10 shows the dependence of the remanence J_r on the average grain size for the irregular (filled signs) and regular (open signs) grain arrangements without α-Fe (solid lines) and with contents of 55% and 51% α-Fe (dashed lines). The remanence always decreases with the grain size. While the numerical results are nearly identical for the irregular and regular microstructure without α-Fe, the irregular grain arrangement with 51% α-Fe and grain diameters above 40 nm leads to small values of J_r of about $0.5J_{sat}$. Obviously, there exist large magnetically soft regions and so the exchange hardening begins to fail.

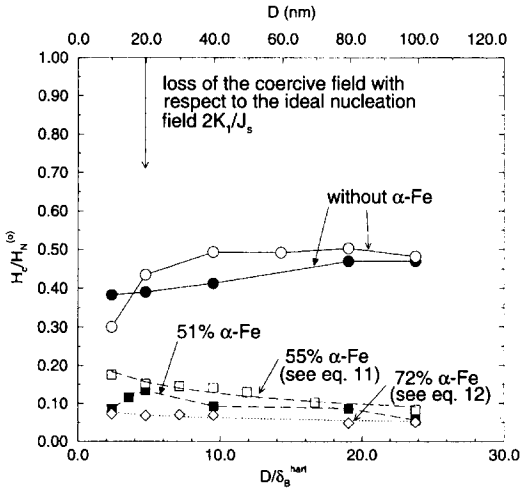

Fig. 11. Reduced coercive field $H_c/H_N^{(0)}$ as a function of the mean grain size,the ideal nucleation field $H_N^{(0)}$ is given by Eq. (16). The filled signs correspond to the irregular grain structures and the open signs to the regular ones.

Large soft regions have a larger chance to escape from the exchange forces exerted by the hard magnetic grains than smaller ones. Whereas the regular microstructure with a mean grain size of about 80 nm shows a remanence enhancement of 10% as compared to the remanent state of noninteracting particles, the remanence enhancement of the irregular grain arrangement vanishes completely.

3.2.2. *Coercive field*

The dependence of the coercive field H_c on the average grain size is presented in Fig. 11 for both grain structures. The irregular structure leads to smaller values of the coercive field for nearly all grain sizes. This may be attributed to the (1) larger soft magnetic regions, and (2) more directly contacted faces between disoriented hard magnetic grains of the irregular grain structure as compared to the uniform one. As pointed out in Section 3.1.2, both microstructural features cause a decrease of the coercive field H_c.

Fig. 11 shows a further interesting phenomena. The coercive field of the irregular grain structure with 51% α-Fe contents increases between 10 and 20 nm and then decreases with the mean grain size. This behaviour can be attributed to the competing effect of the exchange coupling between the soft and the hard magnetic grains as well as the exchange coupling between the hard magnetic grains. This latter exchange coupling leads to an increase of H_c with increasing grain diameter for small grains (see Section 3.1.2.1) whereas the exchange coupling between magnetically soft and hard grains leads to a smooth decrease of H_c with increasing grain diameter (see Section 3.1.2.2).

4. Comparison with experimental results

Fig. 12 compares the numerically calculated values for the remanence and the coercive field with experimental results from Manaf et al. [28] obtained for $Nd_{13.2}Fe_{79.2}B_6Si_{1.2}$ melt-spun ribbons. The numerically calculated values are denoted by circles, whereas experimental values are denoted by plus signs. The numerically obtained grain-size dependence of the magnetic properties is in excellent agreement with the experimentally observed behaviour. On the other hand, although the numerical values of the remanence are only about 0.1 T smaller,

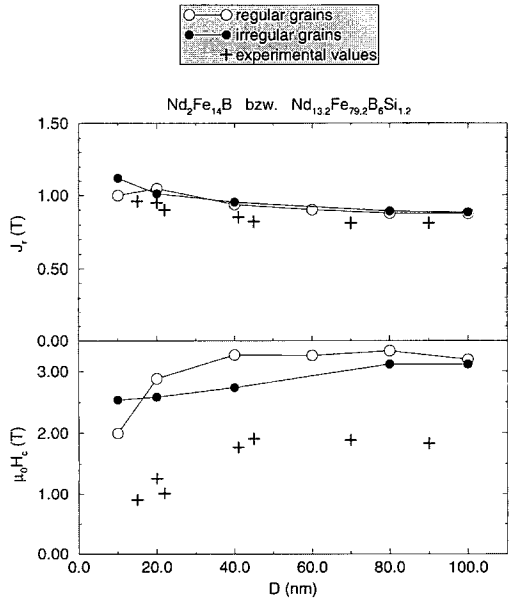

Fig. 12. Remanence J_r and coercive $\mu_0 H_c$ of experimental results from Manaf et al. [28] (plus signs) and numerical obtained values (circles) as function of the mean grain size D. The square belongs to experimental values of a composite magnet obtained by Willcox et al. [6].

those of the coercive field are about 1 T smaller. This behaviour may be attributed to the differences between the theoretical and real grain structures. In permanent magnets, grain boundary phases always exist [29,30]. Such nonferromagnetic phases may cause large local stray fields and therefore a reduction of the coercive field. Furthermore, the present micromagnetic algorithm does not take into account thermally activated processes. Actually, energy barriers may be overcome by thermal activation. Thus, the numerical results will be improved if the grain boundary phases and methods to mimic thermal activations are incorporated into the numerical investigations. Finally, it must be mentioned that permanent magnets consist of thousands of grains. From this point of view, the number of grains of the investigated grain arrangements is very small. But with increasing number of grains, the calculation time increases drastically. A grain arrangement of 64 grains already needs 3 CPU days (Cray-YMP). Since the numerical results of a grain structure with 35 and 64 grains are almost similar [19], we prefer the microstructure with 35 grains. But finally it must be mentioned that finite size effects cannot be completely excluded.

The experimentally investigated grain structures of composite permanent magnets [2–7] consist of soft magnetic grains as small as possible embedded between hard magnetic grains, because large extended soft magnetic regions destroy the coercivity. In Fig. 12, the square belongs to experimental values for a Nd-Fe-B magnet with 35% α-Fe (exact composition: $Nd_8Fe_{86}B_6$) and a mean grain size of about 30 nm, investigated by Willcox et al. [6]. In comparison with Nd-Fe-B magnets without α-Fe, the remanence increases and the coercive field decreases with the soft magnetic volume fraction. This is consistent with the numerical investigations (see Figs. 10 and 11).

5. Summary and conclusions

Micromagnetic calculations show that microstructural features influence the behaviour of isotropic, $Nd_2Fe_{14}B$-based, exchange-coupled composite magnets containing α-Fe. The following sections summaries qualitatively the relation between the important magnetic properties and the average grain size as well as the volume fraction of soft magnetic phase. Furthermore these numerical results will reveal the microstructural conditions required to produce a highly remanent and highly coercive composite material.

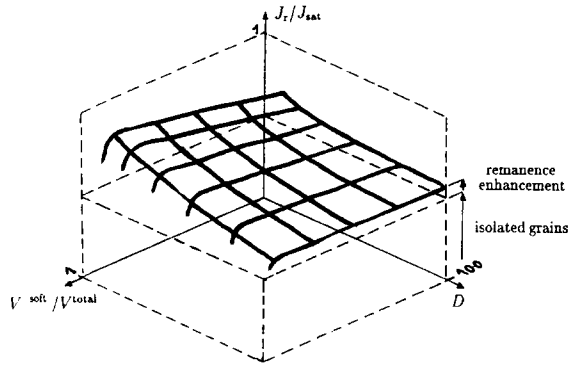

Fig. 13. Reduced remanence J_r/J_{sat} as a function of the mean grain size D and the volume fraction of the soft magnetic phase V^{soft}/V^{total}, the figure shows only the schematic behaviour. The relation between the remanence and the contents of α-Fe has been studied in [19].

5.1. Remanence

The remanence decreases approximately logarithmically with the average grain size and increases approximately linearly with the volume fraction of soft magnetic phase [19]. Fig. 13 shows this behaviour schematically. Interparticle exchange interactions enhance the remanence with respect to isolated particles for a mean grain size approaching twice the domain wall width of the hard magnetic phase and for a significant percentage of α-Fe.

5.2. Coercive field

The coercive field decreases approximately logarithmically with increasing average grain diameter if the volume fraction of soft magnetic phase exceeds 50%. Otherwise, the coercive field first increases at small grain sizes. But with increasing volume fraction of the soft magnetic phase, the coercive field always decreases (see Fig. 14). A numerical micromagnetic analysis shows that strongly inhomogeneous magnetic ground states account for low coer-

cive fields in isotropic nanocrystalline permanent magnets, because of the gain in exchange and crystalline anisotropy energy after magnetization reversal [11]. Thus one can conclude that large local demagnetizing fields near sharp edges and corners of irregular shaped grains, strongly disoriented hard magnetic grains and bad exchange hardening of soft magnetic grains become the crucial effects, which determine the coercive field.

5.3. Guidelines to optimize the grain structure

The numerical results provide the following guidelines to optimize the grain structures of isotropic nanocrystalline permanent magnets:

5.3.1. Hard magnetic materials

In order to achieve a significant remanence enhancement in isotropic nanocrystalline $Nd_2Fe_{14}B$-based magnets, a mean grain size $D < 20$ nm and directly contacted grains without any grain boundary phases are required. In this case, interparticle interactions enhance the remanence by about 35% with respect to isolated particles. With increasing grain diameter the coercive field first increases, but the remanence enhancement decreases (compare Figs. 13 and 14 for $V^{soft}/V^{total} \equiv 0$).

5.3.2. Composite magnetic materials

In order to achieve large coercive fields, in high-remanence composite magnets containing α-Fe, small soft magnetic grains of about 10 nm are required to enforce the exchange hardening. A two-phase magnetic with $D \approx 10$ nm and 55% α-Fe shows a remanence enhancement of about 50% with respect to isolated grains.

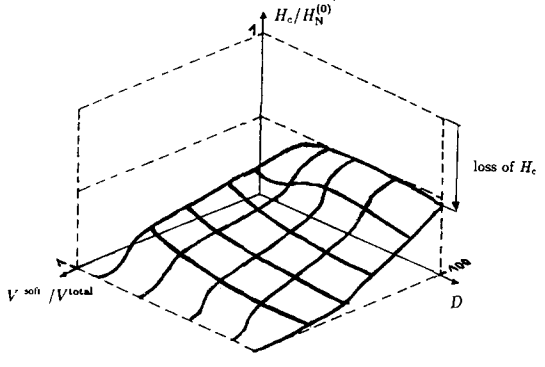

Fig. 14. The same as in Fig. 13, but now for the reduced coercive field $H_c/H_N^{(0)}$.

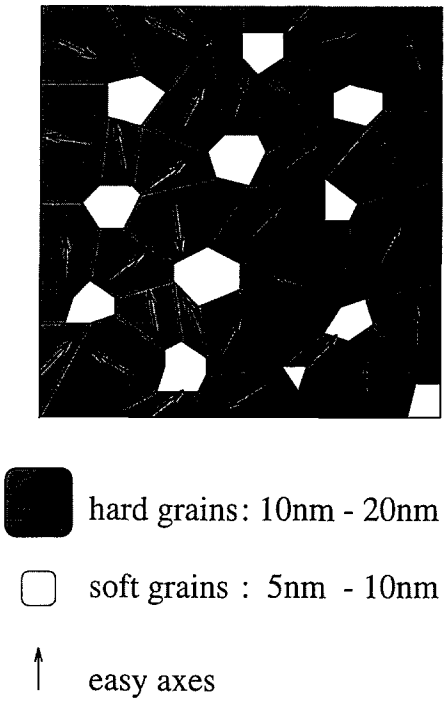

Fig. 15. Schematical cut through a three-dimensional grain arrangement suggesting by the numerical investigations. If small soft magnetic grains are completely surrounded by hard magnetic particles, the α-Fe contents can increased up to 40%. In this case, the remanence enhances and the coercive field preserves sufficiently high.

Fig. 15 shows schematically a cut through a three-dimensional grain structure, which fulfils most of above guidelines.

References

[1] E.F. Kneller and R. Hawig, IEEE Trans. Magn. 27 (1991) 3588.
[2] J. Ding, P.G. McCormick and R. Street, J. Magn. Magn. Mater. 124 (1993) 1.
[3] A. Manaf, R.A. Buckley, H.A. Davies and M. Leonowicz, J. Magn. Magn. Mater. 128 (1993) 302.
[4] A. Manaf, M. Al-Khafaji, P. Zhang, H. Davies, R. Buckley and W. Rainforth, J. Magn. Magn. Mater. 128 (1993) 307.
[5] P. Zhang, M. Al-Khafaji, R. Buckley, W. Rainforth and H. Davies, in: 8th Int. Symposium on Magnetic Anisotropy and Coercivity in Rare Earth–Transition Metal Alloys, Birming-

ham, Sept. 1994, C. Manwaring et al., eds. (University of Birmingham, 1994) p. 249.
[6] M. Willcox, J. Williams, M. Leonowicz, A. Manaf and H. Davies, in: 8th Int. Symposium on Magnetic Anisotropy and Coercivity in Rare Earth–Transition Metal Alloys, Birmingham, Sept. 1994, C. Manwaring et al., eds. (University of Birmingham, 1994) p. 443.
[7] S. Hirosawa and H. Kanekiyo, in: 8th Int. Symposium on Magnetic Anisotropy and Coercivity in Rare Earth–Transition Metal Alloys, Birmingham, Sept. 1994, C. Manwaring et al., eds. (University of Birmingham, 1994) p. 87.
[8] E.C. Stoner and E.P. Wohlfarth, Phil. Trans. Roy. Soc. 240 (1948) 599.
[9] G.B. Clemente, J.E. Keem and J.P. Bradley, J. Appl. Phys. 64 (1988) 5299.
[10] G.C. Hadjipanayis and W. Gong, J. Appl. Phys. 64 (1988) 5559.
[11] T. Schrefl, H. Kronmüller and J. Fidler, Phys. Rev. B 49 (1994) 6100.
[12] T. Schrefl, J. Fidler and H. Kronmüller, J. Magn. Magn. Mater. 138 (1994) 15.
[13] H. Kronmüller, T. Schrefl, R. Fischer and J. Fidler, in: 8th Int. Symposium on Magnetic Anisotropy and Coercivity in Rare Earth–Transition Metal Alloys, Birmingham, Sept. 1994, C. Manwaring et al., eds. (University of Birmingham, 1994) p. 1.
[14] W.F. Brown, Jr., J. Phys. Soc. Jpn. 17 Suppl. B-I (1962) 540.
[15] W.F. Brown, Jr. Micromagnetics (Wiley–Interscience, New York–London, 1963).
[16] H. Kronmüller, Z. für Physik 168 (1962) 478.
[17] H. Kronmüller, in: Moderne Probleme der Metallphysik, A. Seeger, ed. (Springer, Berlin, 1966) Vol. 2, p. 24.
[18] A. Aharoni, IEEE Trans. Magn. 27 (1991) 3539.
[19] R. Fischer, T. Schrefl, H. Kronmüller and J. Fidler, J. Magn. Magn. Mater. 150 (1995) 329.
[20] S. Hock, Ph.D. Thesis, Universität Stuttgart, Germany (1988).
[21] E. Kneller, Ferromagnetismus (Springer, Berlin, 1962).
[22] H. Fukunaga and H. Inoue, Jpn. J. Appl. Phys. 31 (1992) 1347.
[23] A. Hernando, I. Navarro and J.M. Gonzáles, Europhys. Lett. 20 (1992) 175.
[24] T. Schrefl, H.F. Schmidts, J. Fidler and H. Kronmüller, J. Appl. Phys. 73 (1993) 6510.
[25] T. Schrefl, H.F. Schmidts, J. Fidler and H. Kronmüller, IEEE Trans. Magn. 29 (1993) 2878.
[26] A. Sakuma, S. Tanigawa and M. Tokunaga, J. Magn. Magn. Mater. 84 (1990) 52.
[27] T. Schrefl, H. Kronmüller and J. Fidler, J. Magn. Magn. Mater. 127 (1993) 273.
[28] A. Manaf, R.A. Buckley, H.A. Davies and M. Leonowicz, J. Magn. Magn. Mater. 101 (1991) 360.
[29] J.F. Herbst, Rev. Mod. Phys. 63 (1991) 819.
[30] H. Kronmüller, in: Supermagnets, Hard Magnetic Materials, G.J. Long and F. Grandjean, eds. (Kluwer Academic, Dordrecht, 1991) p. 461.